Inorganic Chemistry

Article

pubs.acs.org/IC

High Magnetic Hardness for the Canted Antiferromagnetic, Ferroelectric, and Ferroelastic Layered Perovskite-like $(C_2H_5NH_3)_2[Fe^{II}Cl_4]$

Jing Han,[†] Sadafumi Nishihara,[†,‡,§] Katsuya Inoue,*[,†,‡,§] and Mohamedally Kurmoo*[,§,∥]

[†]Department of Chemistry, Graduate School of Science, Hiroshima University, Higashi Hiroshima, Hiroshima 739-8511, Japan

[‡]Institute for Advanced Materials Research, Hiroshima University & Natural Science Center for Basic Research and Development, Higashi Hiroshima, Hiroshima 739-8511, Japan

[§]Center for Chiral Science, Hiroshima University, 1-3-1, Kagamiyama, Higashi Hiroshima, Hiroshima 739-8526, Japan

[∥]Institut de Chimie de Strasbourg, CNRS-UMR 7177, Université de Strasbourg, 4 rue Blaise Pascal, 67070, Strasbourg, France

Supporting Information

ABSTRACT: An unusual high magnetic hardness for the layered perovskite-like $(C_2H_5NH_3)_2[Fe^{II}Cl_4]$, in addition to its already found canted antiferromagnetism, ferroelasticity, and ferroelectricity, which are absent for $(CH_3NH_3)_2[Fe^{II}Cl_4]$, has been observed. The additional CH_2 in the ethylammonium compared to methylammonium allows more degrees of freedom and therefore numerous phase transitions which have been characterized by single-crystal structure determinations from 383 to 10 K giving the sequence from tetragonal to orthorhombic to monoclinic ($I4/mmm \leftrightarrow P4_2/ncm \leftrightarrow Pccn \leftrightarrow Pcab \leftrightarrow C2/c$) accompanied by both tilting and rotation of the $FeCl_6$ octahedra. The magnetic properties on single crystal and powder samples at high temperature are similar for both compounds, but at T_N $(C_2H_5NH_3)_2[Fe^{II}Cl_4]$ is a proper canted antiferromagnet unlike the hidden canting observed for $(CH_3NH_3)_2[Fe^{II}Cl_4]$. The canting angle is 0.6° toward the *c*-axis, and thus the moments lie in the easy plane of the iron-chloride layer defined by a critical exponent $\beta = 0.18$. The isothermal magnetizations for the field along the three orthogonal crystallographic axes show wider hysteresis for $H \parallel c$ and is present at all temperature below 98 K. The coercive field increases as the temperature is lowered, and at $T < 20$ K it is difficult to reverse all the moments with the available 50 kOe of the SQUID for both single crystal and powder samples. The shape of the virgin magnetization after zero-field-cool (ZFC) indicates that the high coercive field is due to domain wall pinning. Thus, there are unusual associated anomalies such as asymmetric hysteresis and history dependence. The difference in magnetic hardness of the two compounds suggests that magnetic, electric, and elastic domains are intricately manifested and therefore raise the key question of how the different domains interact.

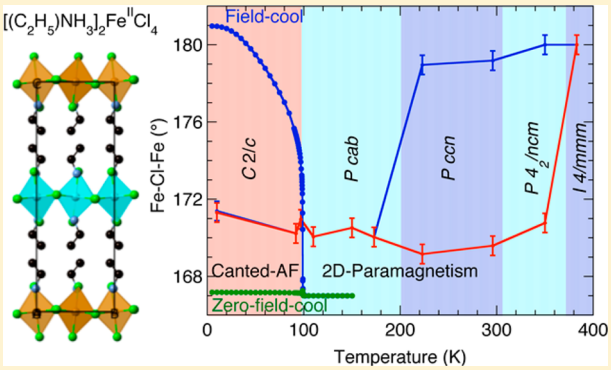

INTRODUCTION

In the past 20−30 years there has been a great purpose in molecular science to marry different physical properties in one single crystalline material, especially metal−organic hybrids due to the possibility of each moiety contributing its own characteristic properties.[1] For example, the coexistence of electrical conductivity and magnetism or optical properties can be beneficial in informatics such as data storage and high-definition screens as well as solar energy conversion.[2] As such, several science communities are developing materials with a variety of combinations of properties. Consequently, much effort is being devoted to understand when, how, and why certain properties are easily coupled and others are not, as well as what is the synergy involved when they do.[3] But most importantly for the chemists is the development of these materials, and this is where metal−organic systems are becoming an exclusive set since the tuning of the organic moiety often has considerable consequence on the structural and physical properties of the inorganic moiety, or vice versa.[4] Among the systems being scrutinized presently are those displaying magnetic, electric, elastic, and toroidic properties—grouped under the heading of "Multiferroic".[5] One such example is $(C_2H_5NH_3)_2[Fe^{II}Cl_4]$, which is a canted antiferromagnet and displays both ferroelectricity and ferroelasticity, while $(CH_3NH_3)_2[Fe^{II}Cl_4]$ exhibits only antiferromagnetism with hidden canting and a low metamagnetic critical field of 200 Oe.[6−8] Following our study of the latter, we studied the structural and magnetic properties of the next member $(C_2H_5NH_3)_2[Fe^{II}Cl_4]$, where in addition to its already reported

Received: December 18, 2014
Published: March 4, 2015

DOI: 10.1021/ic5030229
Inorg. Chem. 2015, 54, 2866−2874

canted-antiferromagnetism we found an exceptional magnetic hardness that renders it highly desirable for durable data storage with operating temperatures (<99 K) above that of liquid nitrogen (77 K).

The recent burst of interests in metal−organic multiferroic materials (those displaying long-range magnetic ordering and ferroelectricity) initiated the present work due to our focus on the effect of Dzyaloshinsky−Moriya interaction in chiral magnets that is also manifested in ferroics.[9−11] The current interests are due to the realization of ferroelectricity and magnetic ordering in some metal−organic systems based on divalent transition metal formate having either a porous diamond structure, $M^{II}_3(HCOO)_3$.solvent, or a perovskite structure, $(CH_3)_2NH_2M^{II}(HCOO)_3$.[12,13] Wang et al. and Gao et al. first reported their syntheses and structural and magnetic properties.[14,15] The observation of ferroelectricity has revived the search for multiferroic in coordination compounds.[16−20] The diamond frameworks were among the first porous metal−organic framework to display porosity and long-range magnetic ordering.[21] The solvents in the channels can be removed without destroying the framework and other solvents were inserted in their place while the framework conforms to the shape, size and hydrogen-bonding properties of the inserted solvents with the host frameworks. The magnetic ground states depend on the electronic and spin configurations of the transition metals and the long-range ordering temperature varies with the solvent in the channels. Kobayashi et al. then reported the dielectric properties of the three-dimensional (3D) diamond metal-formate framework, $M_3(HCOO)_3$·solvent,[12] where an anomaly at high temperature was associated with order−disorder of the solvent. On the basis of previous experiences on metal-oxide perovskites, Cheetham et al. then demonstrated ferroelectricity in the 3D perovskite metal-formate frameworks, where the transition involves ordering of the organic cation at the A-site.[17] This work generated a flurry of activities where several groups have performed related studies on other compounds of this family.[18−20] While these 3D materials exhibit ferroelectricity and ferrimagnetism or canted-antiferromagnetism (CAF), the respective transition temperatures are very far apart, ca. 200 K for the former and below 30 K for the latter. Cheetham and co-workers also showed the coexistence of ferroelastic and magnetic ordering in $[(CH_2)_3NH_2][Mn(HCOO)_3]$, where the cation is the cyclic $[azetidinium]^+$.[22]

Cheetham's reports were also behind reviving the search for multiferroic in metal−organic layered perovskite by Palstra et al., Kundys et al., and Xiong et al.[23−25] Some 30 years earlier these layered perovskite-like compounds, $A_2M^{II}X_4$, where A is an alkyl- or aryl-ammonium cation, M are divalent diamagnetic or paramagnetic metals, and X is a halogen, experienced intense activity due to the long-range magnetic ordering and their multitude of phase transitions.[26−29] Ferroelectric transition has already been reported for the ethylammonium salts of cadmium, iron, and manganese chloride, while Kundys et al. have added the copper chloride to this list, and Palstra et al. reported similar results for propyl ammonium copper chloride.

The results of these recent studies and the observation of spiral spin orders[30] in the oxide perovskite[31] prompted us to study the family of layered perovskite $A_2M^{II}Cl_4$,[32] where A is an alkyl ammonium, M is iron(II) to provide the magnetism, in order to complement our long-term interest in chiral materials.[9−11] These materials have been of major interest since the early seventies due to the long-range magnetic ordering of the moments at fairly high temperatures of ca. 100 K, although they are layered with interlayer spacing of up to 30 Å in some cases. Having realized that the crystal chemistry and the magnetic properties of the $(CH_3NH_3)_2FeCl_4$ (MAFC) are far more complex than those reported,[8] we have now examined the structural and magnetic properties of the ethyl analogue, $(C_2H_5NH_3)_2$·$FeCl_4$ (EAFC), which is supposed to have a weaker interlayer magnetic interaction while maintaining interactions of similar energies within the layer as that of MAFC.

In contrast to MAFC, EAFC has been relatively less studied. Willett et al. reported its Mössbauer spectrum at room temperature to show it exhibits similar parameters for Fe^{II} as MAFC.[6a] Suzuki et al. determined the lattice parameters (a' = 7.314, b' = 7.238, c = 21.90 Å) at room temperature using X-ray oscillation method and located the phase transitions at 97.7, 133.7, 203.5, and 378.8 K using elastic (C_{66}) measurements.[6b] They also demonstrated ferroelastic domain of the order of millimeter using a polarizing microscope and measured the dielectric properties using a capacitance bridge to show the associated anomaly at 203.5 K. In a couple of subsequent papers,[6c,d] Yoshihara et al. proposed the $I4/mmm$−$Cmca$−$Pbca$−$P2_1/a$ sequence of transitions from Brillouin scattering and associated the anomaly at 203 K to a transformation from a D_{2h}^{18} to a D_{2h}^{15} symmetry change with respect to that reported for the structurally characterized cadmium and manganese analogues. In the second paper they theoretically reproduced the temperature dependence dielectric using Landau theory. Using heat capacity data to confirm the four phase transitions at the appropriate temperatures and the critical exponent, Yoshizawa et al. concluded a crossover from XY to Ising at the magnetic transition.

A year after the study of the magnetic properties from 80 to 300 K by Mostafa et al., Nakajima et al. reported the magnetic properties of EAFC to low temperatures where they used a field of 9.5 kOe to determine the remnant magnetization along the c-axis and the perpendicular moment in the plane as a function of temperature. Both groups found a transition temperature near 100 K to a canted antiferromagnetic state, and the latter group estimated a canting angle of 0.63°. Equally low-resolution data have been reported for other iron chloride salts of longer alkyl- or aryl-ammonium.

Following the realization of the intricate balance of energies involved in MAFC,[8] we performed similar magnetization measurements using one aligned single crystal and fields varying from a few Oersted to several kilo Oersted. The results for EAFC are quite different from those of MAFC, which has a hidden-canted antiferromagnetic ground state and metamagnetism in field of 200 Oe along the c-axis. For EAFC the results are consistent with canted-antiferromagnetism along the c-axis. In addition, EAFC exhibits a phenomenal magnetic hardness exemplified by coercive field exceeding 50 kOe as well as a unique metastable state where the magnetic hysteresis of a virgin sample, along all three crystallographic axes, is asymmetric in moment but subsequent loops are symmetric. The hysteresis loop is considerably reduced in powdered samples due to domain effects. The results question the intricate manifestation of the coexistence of elastic, electric, and magnetic domains and their length scales.

EXPERIMENTAL SECTION

Synthesis. Since the product and reactants are hygroscopic and air sensitive, all the steps were carried out in inert N_2 atmosphere. EAFC

DOI: 10.1021/ic5030229
Inorg. Chem. 2015, 54, 2866−2874

was obtained by mixing methanol solutions of ethylammonium chloride, $(C_2H_5NH_3)Cl$, and $FeCl_2{\cdot}4H_2O$ in a 2:1 molar ratio. Clear light ochre plate crystals were obtained by slow crystallization after a few days. The crystals were either kept in sealed containers in the mother liquor or selected and stored under N_2 in the presence of CaO as drying agent.

Thermal Measurements. Thermogravimetric analysis was performed on a SII EXSTAR TG/DTA 6200N from 300 to 600 K at a heating rate of 5 K/min under a nitrogen flow.

Magnetic Susceptibility Measurements. All the magnetic measurements were performed using Quantum Design SQUID magnetometers. The temperature dependence of the magnetic susceptibility was measured between 2 and 400 K in different external fields from 1 to 5000 Oe. Isothermal magnetizations were measured in field between ±50 kOe. ac-susceptibilities were measured with ac-fields from 0.8 to 5 Oe oscillating at different frequencies between 1 and 1000 Hz and dc-field from 0 to 20 Oe. Selected single crystals were fixed on pieces of drinking straw with Araldite. To verify that the crystals had not moved, we embedded crystals in poly(methyl methacrylate) (PMMA) and repeated the measurements along its three axes.[33] Angular dependence magnetization measurements were performed using the Quantum Design rotator. Crystals were indexed using X-ray diffraction prior to use or after the experiments.

Crystallographic Data Collections and Structure Determinations. Seven single crystals from different batches were used for the unit-cell determinations and structure refinements at different temperatures. Typically a single crystal was mounted on a glass fiber. The temperature of the crystal was slowly decreased to that desired or to 90 K (nitrogen flow cryostat) before taking measurements on warming. On two crystals the temperature was cycled from 383 to 90 K and back. One crystal was used in a helium cryostat for structure determinations at 10 and 150 K. Lattice parameters were measured as a function of temperature, and intensity data collections were made at some selected temperatures for which full structural analyses were carried out. All measurements were performed on a Bruker SMART-APEX diffractometer equipped with a CCD area detector and graphite-monochromated Mo Kα radiation, λ = 0.71073 Å, ω-scan mode (0.3° steps). The structures were solved by direct methods and refined by full-matrix least-squares against F^2 of all data using SHELX-97.[34] Non-hydrogen atoms were refined anisotropically. Hydrogen atoms were included with isotropic thermal parameters but not refined.

RESULTS AND DISCUSSION

Thermal Properties. Thermogravimetric analysis shows that EAFC is stable to 450 K where it starts decomposing to give iron oxide.

Crystal Structures and Structural Phase Transitions. A detailed description of the structure of EAFC in all the phases has not been properly reported, although several reports indicate it has a structure similar to that of the manganese analogue.[35] We determined the full structures at different temperatures between 10 and 400 K covering the phase diagram (Figures 1 and 2). From heat capacity, elastic measurements, and single crystal X-ray crystallography, Suzuki et al. have given the following details: tetragonal $I4/mmm$−378 K−orthorhombic $Bmab$ or $Pccn$−203 K−orthorhombic $Fm2m$ or $P4_2/ncm$−133 K−$P2_1/c$−98 K−monoclinic $P2_1/c$.[6b] Although the general trends are the same as our findings, some details are slightly different due to the choice of space groups. First we find $P4_2/ncm$ describes better the structure at 350 K, $Pccn$ for 296 and 223 K (phase II), while the space group, $Pbca$ envelopes phases III and IV between 97 and 173 K. However, due to instability of temperature using the N_2 jet-stream cryostat several data sets around 90 K are less reliable and therefore not used. We used data mostly with reliability $R \leq 0.1$ except in two cases at 97 and 150 K. The structure at 10 K was resolved in $C2/c$ rather than $P2_1/c$ found at 80 K. These phase transitions are associated with both tilting of the octahedra and their rotations about the c-axis that are also accompanied by the continuous rotation of the plane containing the three heavy atoms of the ethylammonium with temperature.

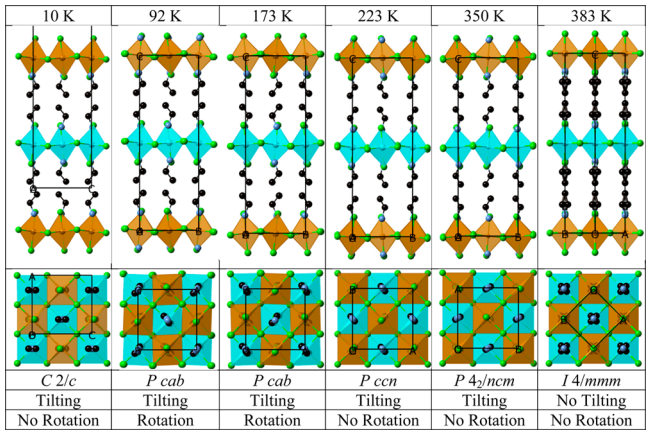

Figure 1. Views of the crystal structures at different temperatures showing the tilting of the octahedra (top) and the rotation of the octahedra and of the cations (bottom).

The key feature of the structure consists of inorganic layers (ab-plane) separated by double layers of organic cations stacked along the c-axis. Each unit cell contains two staggered layers stacked in an $ABAB$ fashion. The distance between two adjacent inorganic planes is ca. 10.5 Å, 1 Å longer than in MAFC.[8] The inorganic layers are made up of corner-sharing octahedra of $FeCl_6$, as that in a perovskite. The octahedra display Jahn−Teller axially compressed distortion where the nonbridging axial chlorine atoms are closer (Fe−Cl1 = 2.41 Å) than the intralayer bridging ones (Fe−Cl2 = 2.54 and Fe−Cl3 = 2.56 Å) to the iron center (Figure 2). The axial chlorine atoms are involved in hydrogen bonds with the ammonium moiety of the organic cations that sandwich the inorganic layer.

The change of the lattice parameters with temperature is smooth within the experimental accuracy and the variance from crystal to crystal (Figure 2a). There seems to be a minimum in all three parameters but that of the c-axis is more pronounced. There is a general marginal increase upon warming. Upon close examination of the results, we find a subtle tilting of the $FeCl_6$ octahedra accompanied by a puckering of the chlorine atoms within the layer from the tetragonal phase to the orthorhombic and monoclinic phases (Figure 2c). In contrast to only the progressive tilting of the octahedra observed for MAFC as the temperature is lowered, for EAFC the tilting is not progressive and there is additionally a rotation of the octahedra.[8] The two effects are concerted, and they are accompanied by the rotation of the plane of the ammonium cation which appears to be progressive from 36° at 383 K to 90° at 10 K (Figure 2d).

The coordination of the iron center is an axially compressed octahedron along the c-axis; that is, the Fe−Cl_{ax} bond length is shorter by 0.25 Å than those of Fe−Cl_{eq} (Figure 2b). On lowering the temperature the difference is reduced to 0.15 Å due to a concerted elongation of Fe−Cl_{eq} and a shortening of Fe−Cl_{ax}. In contrast to what we have shown before for MAFC where the nitrogen atom of the amine follows the two-in two-out tilting of the octahedra progressively as a function of temperature as defined by the supramolecular interactions (N···Cl), in the present case the change happens at the tetragonal to

DOI: 10.1021/ic5030229
Inorg. Chem. 2015, 54, 2866−2874

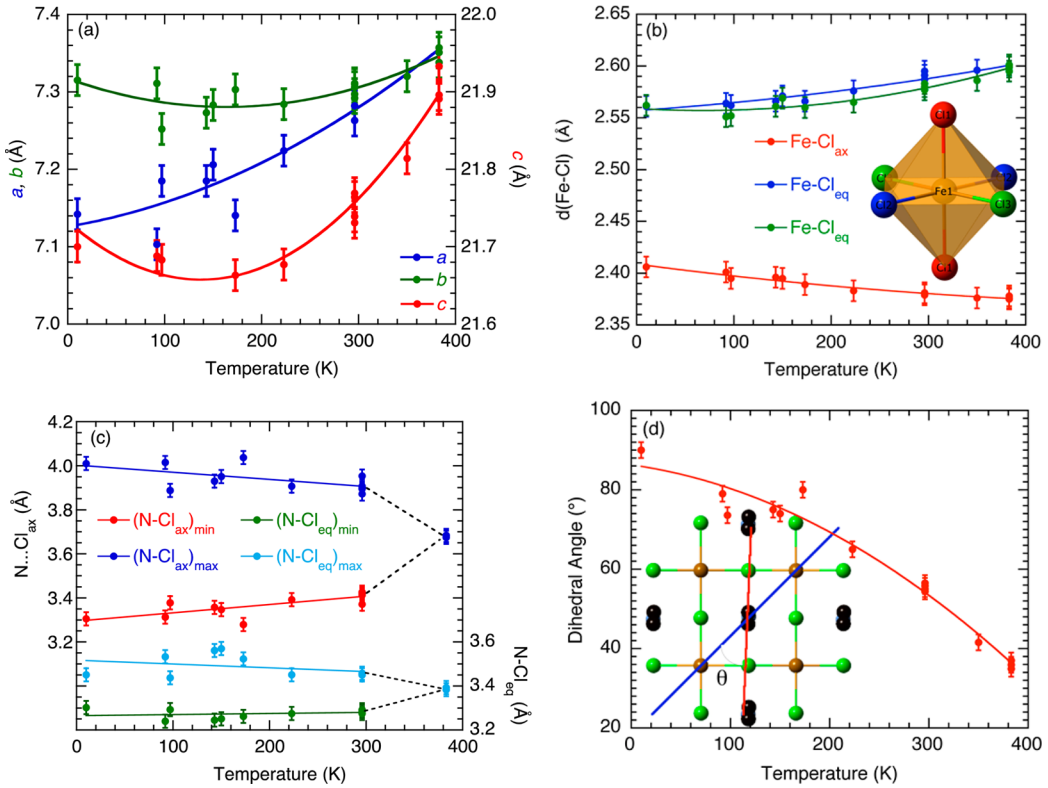

Figure 2. Temperature dependence of the (a) lattice parameters, (b) Fe−Cl bond lengths, (c) minimum and maximum lengths of the N···Cl distances, and (d) dihedral angle (θ) of the plane defining the ammonium atoms (red line) and the Fe−Fe direction (blue line). The lines are all guides to the eyes.

orthorhombic transition at 378 K, and it remains almost constant at low temperatures.

From the parameters discussed above, it is difficult to see a real phase diagram emerging. However, by looking at the Cl−Fe−Cl angles in the equatorial plane one emerges (Figure 3).

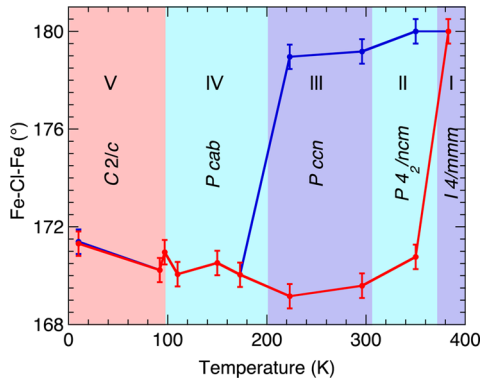

Figure 3. Temperature dependence of the Cl−Fe−Cl equatorial angles within the layer−defining the five phases of EAFC. The blue and red points represent the two different angles and the lines are guides to the eyes.

At 383 K the angles are 180° as imposed by symmetry. Between 350 and 203 K (phase II) there are two different angles where one is nearly 180° and the other ca. 169°. The tilting of the octahedra at 350 and 296 K are along a Cl−Fe−Cl direction with two opposite ones of a Fe_4-square being parallel to one another but antiparallel to the other pair. Instead between 223 and 10 K, the tilting is offset from the Cl−Fe−Cl directions but retain the pairwise configuration. The angles become similar (170 ± 1°) in phase III. In the structure taken at the magnetic transition (97 K), the angles revert which may be due to the magnetostriction effect (the set of data at 97 K is not well refined and the results are of low quality). Finally at the lowest temperature of 10 K the monoclinic structure results in similar angles of 171.3(1)°.

Magnetic Properties and Magnetic Phase Transition. With the experience acquired during the study of MAFC we decided to perform magnetic measurements on both single crystals and powders.[8] Numerous powdered samples in gelatin capsules and five crystals were studied independently while being fixed on strip of drinking straw. To verify these results we later studied two more crystals embedded in PMMA.[33] For the latter it was easier to manipulate the crystals in between experiments and also to keep them for further experiments after longer periods as they are protected from air oxidation.

The behaviors of the magnetic susceptibilities for field along the three orthogonal crystallographic axes show a broad maximum at ca. 150 K (Figure 4). The absolute value of the susceptibility follows the trend $H \parallel a \sim H \parallel b > H \parallel c$. The data are consistent with those observed for MAFC. Analyses of the high temperature data (250−400 K) using the Curie−Weiss function give very large Weiss temperatures (−300 ± 5 K for $H \parallel a$ or b and −530 ± 10 K for $H \parallel c$). From the Curie constants we found the following g-value relation, $g_a/g_b/g_c$ = 1:1:1.175. The broad maximum centered around 150 K in each case is characteristic of the two-dimensional antiferromagnetic behavior.[35,36] The values of the Weiss temperature suggest very strong antiferromagnetic interaction between nearest iron centers within the layer. However, the very large value of −530 K does not reflect the true exchange interactions between

DOI: 10.1021/ic5030229
Inorg. Chem. 2015, 54, 2866−2874

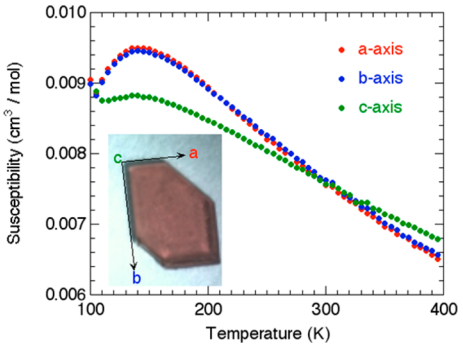

Figure 4. Temperature dependence of the susceptibility (M/H) of a single crystal embedded in PMMA for H = 5 kOe || a-axis (red), || b-axis (blue) and || c-axis (green) in the paramagnetic region 100−400 K.

nearest neighbors and between layers due to the limiting temperature range used for the estimation that are lower than the estimated exchange interaction. Considering the crystal structure, where the layers are not chemically connected to one another and are 11 Å apart, we expect the exchange to be dipolar and thus very small with respect to those within the layer where the connection is through one chlorine atom bridge.

There were no anomalies in the susceptibility data for all three axes that can be associated with the aforementioned structural transitions at 378, 203, and 133 K, but at the 99 K magnetic transition a sharp increase in magnetization is observed along all three axes which slowly tends to saturation at low temperatures when cooled in field and that for H || c is the most pronounced (Figure 5). The small magnetization for

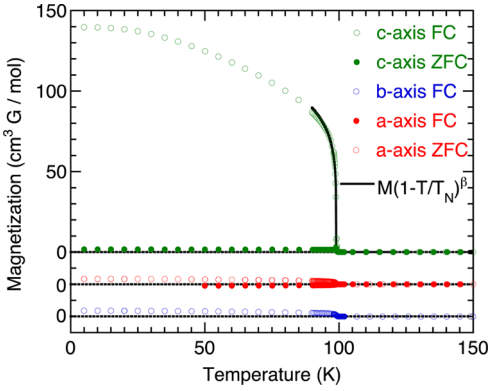

Figure 5. Temperature dependence of the zero-field-cool and field-cool magnetizations of a single crystal embedded in PMMA in an applied field of 1 Oe for H || a-axis (red), || b-axis (blue) and || c-axis (green) in the region 5−150 K. The slight negative ZFC magnetization for H || b-axis is due to a negative field of <0.1 Oe on cooling. The black line is the fit for the critical exponent.

H || ab plane may originate from slight misalignment of the crystals. The zero-field cooled data are very difficult to measure using a squid magnetometer equipped with a 50 kOe magnet, since the smallest field of 0.1 Oe can drive a large magnetization on cooling and the high coercivity of this material (see later) makes it hard to reverse the induced magnetization from say negative to positive. After careful elimination of the trapped field within the shield and that of the magnet coil, a nonzero temperature independent magnetization is observed up to a fraction of a Kelvin from the transition temperature. We manage this once for measurement in an applied field of 1 Oe when H || c-axis. The attempt for H || b was not successful as a very small negative residual field (<0.1 Oe) drove the magnetization to the opposite direction and upon warming in 1 Oe it remains negative until just below T_N. Upon subsequent cooling the increase in magnetization is observed near 99 K but the following remnant magnetization, after removing the field, is nearly the same as the FC data except for the slight shift in the temperature at which the magnetization is zero (Figure 6).

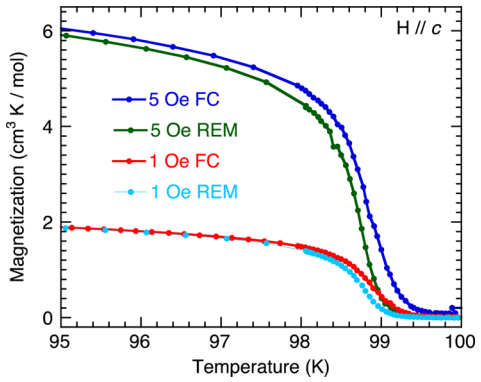

Figure 6. Temperature dependence of the field-cool and remnant magnetizations of a single crystal embedded in PMMA in applied fields of 1 and 5 Oe for H || c-axis.

This effect is also seen for data taken in 5 Oe field and it appears to be for any orientations and for different crystals. The magnetization data taken in 50 Oe are as those reported above for 1 and 5 Oe. However, if presented as susceptibility there is large variance indicating the initial susceptibility is nonlinear. The FC magnetization data measured in 1 and 5 Oe for H || c have been fitted to $M = M_0(1 - T/T_N)^\beta$ to extract the critical exponent (Figure 5).[37] The Néel temperature was found to be 98.9(1) K and the critical exponent β = 0.180(2).

Increasing the applied field to 100 and 500 Oe, the ZFC data change shape by becoming broader with increasing field but the bifurcation between ZFC and FC data remains for all temperatures below 90 K (Figure 7). We note that the magnetization in 50, 100, and 500 Oe tend to the same value. For applied fields of 5 and 10 kOe a very sharp rise is observed in the ZFC magnetization below 10 K, but the difference between ZFC and FC is still present. In 20 kOe the sharp increase is absent. The FC magnetization value at 2 K depends on the applied field up to 50 Oe and reaches the same value for field strength of 50, 100, and 500 Oe. At higher fields, 5, 10, and 20 kOe, the saturation value is again dependent on the applied field but is nonlinear. However, in each of the applied fields used the value of the magnetization at 2 K is very far from that expected for a ferromagnetic material with all moments parallel, suggesting a canted-antiferromagnetic ground state is most appropriate. The dependence of the magnetization for fields of 1−50 Oe is likely to be due to the motion of domains, but the nonlinearity may be associated with their highly 2D nature. The same saturation magnetization values (250 cm^3 G/mol) for H = 50−500 Oe reflect the canting moment of this magnet. Thus, taking the value of 250 cm^3 G/mol for the magnetization at 2 K in 50 Oe and using gS = 2*2*5585 cm^3 G/mol for a fully aligned Fe(II) moment, we estimate the canting angle as $\sin^{-1}[250/(2*2*5585)]$ = 0.64°. This is the

DOI: 10.1021/ic5030229
Inorg. Chem. 2015, 54, 2866−2874

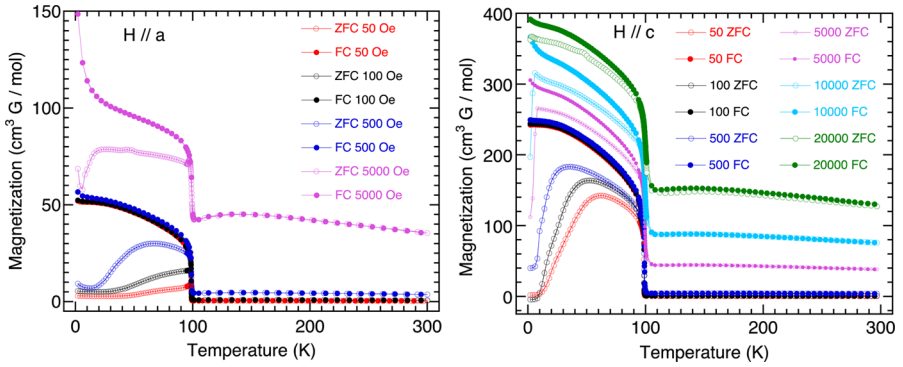

Figure 7. Temperature dependence of the zero-field-cool and field-cool magnetizations of a single crystal in different applied fields $H \parallel a$-axis (left) and $H \parallel c$-axis (right).

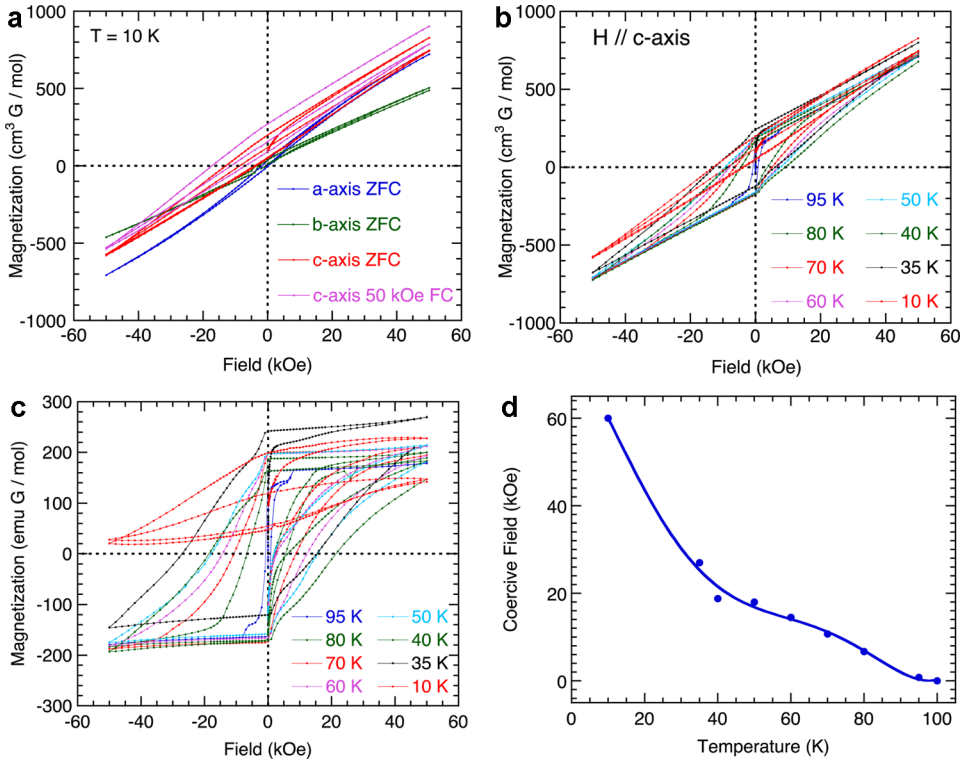

Figure 8. (a) Isothermal magnetization at 10 K of a single crystal embedded in PMMA after zero-field-cool for $H \parallel a$-axis (blue), $\parallel b$-axis (blue), and $\parallel c$-axis (green) and after field cooling in 50 kOe from 300 K for $H \parallel c$-axis (purple). (b) Isothermal magnetization at different temperatures for a single crystal after zero-field-cool with $H \parallel c$-axis. (c) Isothermal magnetization at different temperatures for a single crystal after zero-field-cool with $H \parallel c$-axis after removal of a linear part (see text). (d) Temperature dependence of the coercive field for a single crystal after zero-field-cool with $H \parallel c$-axis.

same as that found by Nakajima et al.[6e] However, the nonlinear susceptibility in field of 5−20 kOe suggests reversal of moments, which is rarely found for a canted-antiferromagnet. Its origin in the present case is presently not known.

The above observations are indication that it is difficult to move the domain walls in this compound, and thus it is very coercive and hard. However, the rapid reversal in low field after ZFC suggests the mechanism for the magnetic hardness is due to wall pinning rather than nucleation driven (Figure 8).[38] In contrast to the soft nature of MAFC that does not display any electric or elastic properties, the magnetic hardness in the present case raises the question of the manifestation of the coexistence of the different domains of varying length scales and the relation between them. As expected the magnetic hardness is increased in the powdered samples (Figure S1) due to reduction of multidomains further questions how the three properties are intricately connected. The results from several crystals were consistent and reproducible irrespective of their size (1−3 mm), shape, and the method of crystal mounting used.

The ac-susceptibilities of this compound are very sensitive to the ac- and dc-field as well as the oscillating frequency (Figure 9). All measurements were performed on an aligned single crystal. As the susceptibility is highest for field applied parallel to the c-axis, we have aligned the crystal in this orientation. The ac field was chosen from 0.8 to 5 Oe and oscillating frequencies from 1 to 1000 Hz, while the bias dc field was from 0.8 to 20 Oe. First the sample was cooled in zero dc-field and the bias dc field was applied when the temperature has stabilized at 2 K for about 5 min. Thus, the experiment can give us information on

DOI: 10.1021/ic5030229
Inorg. Chem. 2015, 54, 2866−2874

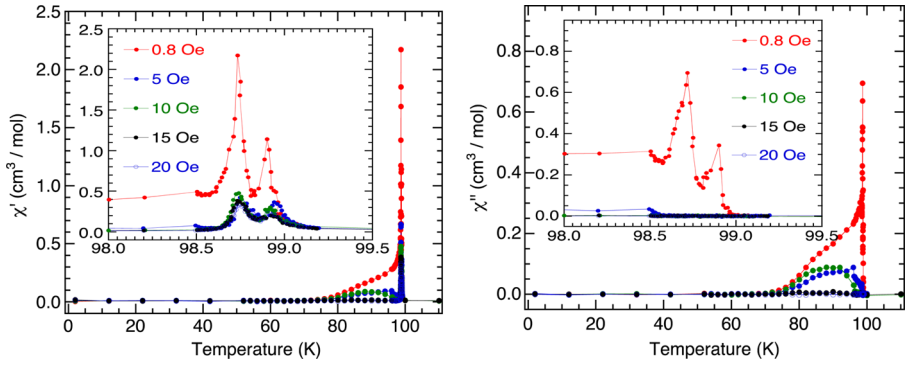

Figure 9. Temperature dependence of the ac-susceptibilities for $H \parallel c$, real part (left) and imaginary part (right); H_{ac} = 0.8 Oe, frequency = 10 Hz and bias dc-field indicated in the figure.

the domain structure and the phase transition. The observed ac-susceptibilities have three anomalies. Below 50 K both the real and imaginary components are very weak or zero. This is consistent with the high magnetic hardness mentioned above. Above 50 K a broad hump is seen which is due to domain wall dynamics, and the other anomaly is two sharp peaks near the Néel temperature. First we found that increasing either the ac- or dc-field independently or simultaneously can have dramatic changes in the response. Both have the effect of decreasing the imaginary component to zero and also the broad hump. The two sharp peaks are centered at 98.9 and 98.7 K. There is very little frequency dependence in the peak temperature, but the intensity decreases with increasing frequency for the real component and the imaginary component becomes zero. We should note that the higher temperature peak matches the transition measured by the field-cool magnetization in 1 or 5 Oe (Figure 6), while the lower temperature peak matches that at which the remnant magnetization becomes zero. The presence of peaks in ac-susceptibilities of canted antiferromagnets is unusual; thus in the present case we associate these anomalies to domain structure within the layer for the weak ferromagnetic state. As we have already argued in the case of methylammonium iron chloride that long-range ordering is prominent in 2D before 3D at a slightly lower temperature, we believe similar conclusion can be drawn in the present case.[8] Although there is a big difference in ground state between the two compounds, the ac-susceptibility behavior is expected to be the same. The varying value of susceptibility for different ac fields is due to the large variation of the initial magnetization as a function of field while the appearance or not of an imaginary part is due to the narrow range of relaxation rate for the canted antiferromagnetism as well as the small width of the domain wall which should lie between that of Bloch for a ferromagnet and that of Néel for an antiferromagnet.[39] It is important to note that with such a narrow peak in the ac-susceptibilities spanning only 0.5 K it is a lesson to learn that one can easily miss these details for canted antiferromagnets and wrong interpretations can follow.

The structural and magnetic data for EAFC shown above present certain anomalies that were not encountered in the studies of MAFC.[8] First in addition to the tilting of the octahedra, there was their rotations within the layer of EAFC that was not present for MAFC and has been associated with the presence of ferroelasticity in EAFC.[6b] Second, the magnetic ground state is different; EAFC is a straight canted antiferromagnet without the hidden canting found in MAFC. The transition temperatures being almost the same suggest that the exchange interactions within the layer are of the same order of magnitude and that a dipole−dipole interaction between layers is the most logical mechanism for the long-range ordering, although the resultant moment due to the canting is smaller (0.64° for EAFC and 1.4° for MAFC).[6e]

The major differences between the two compounds lie in the ac-susceptibilities in the ordered state below the transition temperature, and the hysteresis where both observables are related to magnetic anisotropy. Given the global structural similarity and the mechanism of the long-range ordering being also of the same origin, it leaves us with little reasons not to think of the interaction of domains of different origins—ferroelectric, ferroelastic and ferromagnetic—as being responsible for the various anomalies that are present. In the following we attempt to relate these anomalies.

The most notable anomaly is the large hysteresis which starts to be quite narrow near the transition temperature but grows rapidly as the temperature is lowered to the point where the 50 kOe of the SQUID was not enough to reverse the moments (Figure 8), as seen by the asymmetric loop offset to the upper side (especially at 2 K). Furthermore, the hysteresis of a virgin sample is different from the subsequent ones that are reproducible (Figures S2 and S3, Supporting Information). To envisage the effect it is better to look at the first magnetization and its demagnetization. The former is almost linear and increases rapidly with field up to 1.5 kOe before taking a more gentle increase up to 50 kOe. On decreasing the field the slope is almost the same as the increase in field with a kink at the remnant magnetization point (i.e., at zero field), but the saturation value is drastically reduced at −50 kOe. However, on going back from −50 kOe to +50 kOe the saturation value is the same as that in −50 kOe. To verify that this is not a polar effect we did the reverse, that is, going to the negative field after ZFC and back and forth. The symmetry of the traces is reproduced, suggesting this is not a polar effect. Examination of the loops for $H \parallel c$ at different temperatures indicates the effect is present for every loop below 80 K but not for the one at 95 K (Figure 8c). For all temperatures between 35 and 95 K, the linear component of the magnetization is reproduced following $M = (M_0 + 0.0106\ H)$ emu G/mol. The hysteresis loops at 10 K for the other orientations show the effect is the same but reduced in magnitude. In a powder, the hysteresis is weak but that after FC with positive or negative field are not reversible due to probably enhancement of the coercive field by reducing the particle size. It is to be noted that the difference between virgin and subsequent loops are again not of the same values.

DOI: 10.1021/ic5030229
Inorg. Chem. 2015, 54, 2866−2874

Such kind of magnetic behaviors are unique to EAFC, and in comparison to its sister one MAFC one can presently only associate them with the only difference between them—that is the former is ferroelectric, ferroelastic, and weak ferromagnetic in zero field, while the latter do not display ferroelectric and ferroelastic but weak ferromagnetism in field higher than 200 Oe.[8] Therefore, we tentatively associate the difference between virgin magnetization and subsequent hysteresis to the different scales of the domain size as well interaction between them.

CONCLUSION

Although $(C_2H_5NH_3)_2FeCl_4$ has the same structural characteristics as $(CH_3NH_3)_2FeCl_4$, the extra CH_2 adds to a multitude of phase transitions giving rise to ferroelectric and ferroelastic properties in the former but absent in the latter. The crystal structure determinations point to both tilting and rotation of the octahedra where the latter is associated with the elasticity. The magnetic order is consistent with weak ferromagnetism due to the canting of the moments by 0.64° toward the *c*-axis. In contrast to $(CH_3NH_3)_2FeCl_4$, $(C_2H_5NH_3)_2FeCl_4$ displays wide hysteresis below T_C (98.9 K) which increases dramatically as the temperature is lowered to exceed 50 kOe coercive field. It is among the hardest molecular magnet known. The difference in behavior is tentatively associated with the interaction of domains of electric, elastic, and magnetic origins that have different length scales. How the interaction is manifested remains a question of major scientific curiosity and can only be answered by the presently nontrivial engineering of materials with known domain structures.

ASSOCIATED CONTENT

Supporting Information

Crystallographic information files; isothermal magnetization plot. This material is available free of charge via the Internet at http://pubs.acs.org.

AUTHOR INFORMATION

Corresponding Authors

*(K.I.) E-mail: kxi@hiroshima-u.ac.jp.
*(M.K.) E-mail: kurmoo@unistra.fr.

Notes

The authors declare no competing financial interest.

ACKNOWLEDGMENTS

This work was supported by Grant-in-Aid (JSPS Fellows No. 206688, Scientific Research-A No. 18205023, Scientific Research-S No. 25220803, and Exploratory Research No. 19655050) from the Ministry of Education, Culture, Sports, Science and Technology (MEXT), a "Nanotechnology Support Project" of MEXT and the Natural Science Center for Basic Research and Development (N-BARD), Hiroshima University. J.H. thanks Monkasho for a JASSO student scholarship. M.K. thanks the CNRS, France, and Hiroshima University for a Honorary Professorship at the Center for Chiral Material, Hiroshima.

REFERENCES

(1) (a) Day, P. *Molecules into Materials: Case Studies in Materials Chemistry – Mixed Valency, Magnetism and Superconductivity*; World Scientific Publishing: Singapore, 2007; pp 1–604. (b) Day, P.; Gillespie, R. *Philos. Trans. R. Soc. London* **1985**, *A314*, 1–198. (c) Day, P.; Underhill, A. E. *Metal-Organic and Organic Molecular Magnets*; Royal Society of Chemistry: Cambridge, U.K., 1999; pp 1–324. *Phil. Trans. R. Soc. London*, **1999** vol. *357*. (d) Long, J. R.; Yaghi, O. *Chem. Soc. Rev.* **2009**, *38*, 1213–1504. (e) Sadakiyo, M.; Yamada, T.; Kitagawa, H. J. *Am. Chem. Soc.* **2009**, *131*, 9906–9907.

(2) (a) Kurmoo, M.; Graham, A. W.; Day, P.; Coles, S. J.; Hursthouse, M. B.; Caulfield, J. L.; Singleton, J.; Pratt, F. L.; Hayes, W.; Ducasse, L.; Guionneau, P. J. *Am. Chem. Soc.* **1995**, *117*, 12209–12217. (b) Coronado, E.; Galan-Mascaros, J. R.; Gomez-Garcia, C. J.; Laukhin, V. *Nature* **2000**, *408*, 447–449. (c) Uji, S.; Shinagawa, H.; Herashima, T.; Yakabe, T.; Terai, Y.; Tokumoto, M.; Kobayashi, A.; Kobayashi, H. *Nature* **2001**, *410*, 908–910. (d) Marchioro, A.; Teuscher, J.; Friedrich, D.; Kunst, M.; van de Krol, R.; Moehl, T.; Gratzel, M.; Moser, J.-E. *Nat. Photonics* **2014**, *8*, 250–255. (e) Tokura, Y.; Seki, S. *Adv. Mater.* **2010**, *22*, 1554–1565.

(3) Blundell, S. J.; Pratt, F. L. *J. Phys.: Condens. Matter* **2004**, *16*, R771–R828.

(4) (a) Cox, P. A. In *Solid State Chemistry: Compounds*; Cheetham, A. K.; Day, P., Eds.; Clarendon Press: Oxford, 1992; pp 1–30. (b) Jacobsen, A. J. Intercalation Reactions of Layered Compounds. In *Solid State Chemistry: Compounds*; Day, P.; Cheetham, A., Eds.; Oxford University Press: Oxford, 1992; pp 182–200.

(5) (a) van den Brink, J.; Khomskii, D. I. *J. Phys.: Condens. Matter* **2008**, *20*, 434217/12. (b) Fiebig, M. *J. Phys. D: Appl. Phys.* **2005**, *38*, 123–152. (c) Cheong, S. W.; Mostovoy, M. *Nat. Mater.* **2007**, *6*, 13–20. (d) Hill, N. A. *J. Phys. Chem. B* **2000**, *104*, 6694–6709. (e) Ramesh, R. *Nature* **2009**, *46*, 1218–1219. (f) Eerenstein, W.; Mathur, N. D.; Scott, J. F. *Nature* **2006**, *442*, 759–765.

(6) (a) Mostafa, M. F.; Willett, R. D. *Phys. Rev. B* **1971**, *4*, 2213–2214. (b) Suzuki, T.; Nakajima, H.; Yamaguchi, T.; Goto, M.; Yoshizawa, T.; Suzuki, T.; Fujimura, T. *J. Magn. Magn. Mater.* **1983**, *31–34*, 1189–1190. (c) Yoshizawa, M.; Suzuki, T.; Goto, T.; Yamakami, T.; Fujimura, T.; Nakajima, T.; Yamauchi, H. *J. Phys. Soc. Jpn.* **1984**, *53*, 261–269. (d) Yoshizawa, Y.; Goto, T.; Fujimura, T. *Phys. Rev. B* **1982**, *26*, 1499–1502. (e) Goto, T.; Yoshizawa, M.; Tamaki, A.; Fujimura, T. *J. Phys. C* **1982**, *15*, 3041–3052. (f) Suzuki, T.; Yoshizawa, M.; Goto, T.; Yamakami, T.; Takahashi, M.; Fukimura, T. *J. Phys. Soc. Jpn.* **1983**, *52*, 1669–1675. (g) Baettig, P.; Oguchi, T. *J. J. Appl. Phys.* **2010**, *49*, 080206/3. (h) Yoshihara, A.; Suzuki, T.; Yamakami, T.; Fujimura, T. *J. Phys. Soc. Jpn.* **1985**, *54*, 3376–3384. (i) Yoshihara, A.; Suzuki, T.; Fujimura, T. *J. Phys. Soc. Jpn.* **1985**, *54*, 4607–4620.

(7) (a) Mitzi, D. B. *J. Chem. Soc., Dalton Trans.* **2001**, 1–12. (b) Guo, L.; Liu, H.; Dai, Y.; Ouyang, S. *J. Phys. Chem. Solids* **2007**, *68*, 1663–1673. (c) Knorr, K.; Jahn, I. R.; Heger, G. *Solid State Commun.* **1974**, *15*, 231–238. (d) Heger, G.; Mullen, D.; Knorr, K. *Phys. Status Solidi A* **1976**, *35*, 627–637. (e) Geick, R.; Strobel, K. *J. Phys. C* **1977**, *10*, 4221–4239. (f) Arend, H.; Hofmann, R.; Waldner, F. *Solid State Commun.* **1973**, *13*, 1629–1632. (g) Mostafa, M. F.; Semary, M. A.; Ahmed, M. A. *J. Magn. Magn. Mater.* **1980**, *15–18*, 448–450. (h) Mostafa, M. F.; Semary, M. A.; Ahmed, M. A. *Phys. Lett.* **1977**, *61A*, 183–184. (i) Mostafa, M. F.; Willett, R. D. *Phys. Rev. B* **1971**, *4*, 2213–2214. (j) Willett, R. D.; Gerstein, B. G. *Phys. Lett.* **1973**, *44A*, 153–154. (k) Nakajima, T.; Yamaguchi, H.; Goto, T.; Yoshizawa, M.; Suzuki, T.; Fujimura, T. *J. Magn. Magn. Mater.* **1983**, *31–34*, 1189–1190.

(8) Han, J.; Nishihara, S.; Inoue, K.; Kurmoo, M. *Inorg. Chem.* **2014**, *53*, 2068–2075.

(9) Kumagai, H.; Inoue, K. *Angew. Chem., Int. Ed.* **1999**, *38*, 1601–1603.

(10) Inoue, K.; Imai, H.; Ghalsasi, P. S.; Kikuchi, K.; Ohba, M.; Okawa, H.; Yakhmi, J. V. *Angew. Chem., Int. Ed.* **2001**, *40*, 4242–4245.

(11) (a) Inoue, K.; Kikuchi, K.; Ohba, M.; Ōkawa, H. *Angew. Chem., Int. Ed.* **2003**, *42*, 4810–4813. (b) Imai, H.; Inoue, K.; Kikuchi, K.; Yoshida, Y.; Ito, M.; Sunahara, T.; Onaka, S. *Angew. Chem., Int. Ed.* **2004**, *43*, 5618–5621. (c) Imai, H.; Inoue, K.; Kikuchi, K. *Polyhedron* **2005**, *24*, 2808–2812. (d) Yoshida, Y.; Inoue, K.; Kurmoo, M. *Inorg. Chem.* **2009**, *48*, 10726–10736. (e) Higashikawa, H.; Okuda, K.; Kishine, J.; Masuhara, N.; Inoue, K. *Chem. Lett.* **2007**, *36*, 1022–1023. (f) Kishine, J.; Inoue, K.; Yoshida, Y. *Prog. Theoret. Phys. Suppl.* **2005**,

DOI: 10.1021/ic5030229
Inorg. Chem. 2015, 54, 2866–2874

159, 82−95. (g) Numata, Y.; Inoue, K.; Baranov, N.; Kurmoo, M.; Kikuchi, K. *J. Am. Chem. Soc.* **2007**, *129*, 9902−9909.
(12) Wang, Z.; Zhang, B.; Zhang, Y.; Kurmoo, M.; Liu, T.; Gao, S.; Kobayashi, H. *Polyhedron* **2007**, *26*, 2207−2215.
(13) (a) Wang, Z.; Zhang, B.; Otsuka, T.; Inoue, K.; Kobayashi, H.; Kurmoo, M. *Dalton Trans.* **2004**, 2209−2216. (b) Wang, X. Y.; Gan, L.; Zhang, S. W.; Gao, S. *Inorg. Chem.* **2004**, *43*, 4615−4625.
(14) (a) Wang, Z.-M.; Zhang, B.; Inoue, K.; Fujiwara, H.; Otsuka, T.; Kobayashi, H.; Kurmoo, M. *Inorg. Chem.* **2007**, *46*, 437−445. (b) Hu, K.-L.; Kurmoo, M.; Wang, Z.-M.; Gao, S. *Chem.—Eur. J.* **2009**, *15*, 12050−12064. (c) Wang, X. Y.; Wang, Z. M.; Gao, S. *Chem. Commun.* **2007**, 1127−1129. (d) Xu, G. C.; Ma, X. M.; Zhang, L.; Wang, Z.-M.; Gao, S. *J. Am. Chem. Soc.* **2010**, *132*, 9588−9590.
(15) (a) Wang, Z.-M.; Zhang, B.; Fujiwara, H.; Kobayashi, H.; Kurmoo, M. *Chem. Commun.* **2004**, 416−417. (b) Wang, Z.-M.; Zhang, B.; Kurmoo, M.; Green, M. A.; Fujiwara, H.; Otsuka, T.; Kobayashi, H. *Inorg. Chem.* **2005**, *44*, 1230−1237. (c) Wang, Z.-M.; Zhang, Y.; Kurmoo, M.; Liu, T.; Vilminot, S.; Zhao, B.; Gao, S. *Aust. J. Chem.* **2006**, *59*, 617−628. (d) Zhang, B.; Wang, Z.-M.; Kurmoo, M.; Gao, S.; Inoue, K.; Kobayashi, H. *Adv. Funct. Mater.* **2007**, *17*, 577−585. (e) Wang, Z.-M.; Zhang, Y.; Liu, T.; Kurmoo, M.; Gao, S. *Adv. Funct. Mater.* **2007**, *17*, 1523−1536. (f) Wang, Z. M.; Zhang, B.; Zhang, Y. J.; Kurmoo, M.; Liu, T.; Gao, S.; Kobayashi, H. *Polyhedron* **2007**, *26*, 2207−2215. (g) Hu, K. L.; Kurmoo, M.; Wang, Z.; Gao, S. *Chem.—Eur. J.* **2009**, *15*, 12050−12064.
(16) (a) Cui, H.; Zhou, B.; Long, L. S.; Okano, Y.; Kobayashi, H.; Kobayashi, A. *Angew. Chem., Int. Ed.* **2008**, *47*, 3376−3380. (b) Cui, H. B.; Wang, Z. M.; Takahashi, K.; Okano, Y.; Kobayashi, H.; Kobayashi, A. *J. Am. Chem. Soc.* **2006**, *128*, 15074−1575. (c) Zhang, R.; Xu, G. C.; Wang, Z. M.; Gao, S. *Chem.—Eur. J.* **2013**, *20*, 1146−1158.
(17) (a) Jain, P.; Dalal, N. S.; Toby, B. H.; Kroto, H. W.; Cheetham, A. K. *J. Am. Chem. Soc.* **2008**, *130*, 10450−10451. (b) Jain, P.; Ramachandran, V.; Clark, R. J.; Zhou, H. D.; Toby, B. H.; Dalal, N. S.; Kroto, H. W.; Cheetham, A. K. *J. Am. Chem. Soc.* **2009**, *131*, 13625−13627. (c) Besara, T.; Jain, P.; Dalal, N. S.; Kuhns, P. L.; Reyes, A. P.; Kroto, H. W.; Cheetham, A. K. *Proc. Nat, Acad. Science* **2011**, *108*, 6828−6832. (d) Stroppa, A.; Jain, P.; Barone, P.; Marsman, M.; Perez-Mato, J. M.; Cheetham, A. K.; Kroto, H. W.; Picozzi, S. *Angew. Chem., Int. Ed.* **2011**, *50*, 5847−5850. (e) Thomson, R. I.; Jain, P.; Cheetham, A. K.; Carpenter, M. A. *Phys. Rev. B* **2012**, *86*, 214304/7. (f) Li, W.; Probert, M. R.; Kosa, M.; Bennett, T. D.; Thirumurugan, A.; Burwood, R. P.; Parinello, M.; Howard, J. A. K.; Cheetham, A. K. *J. Am. Chem. Soc.* **2012**, *134*, 11940−11943. (g) Kosa, M.; Tan, J. C.; Merrill, C. A.; Krack, M.; Cheetham, A. K.; Parinello, M. *ChemPhysChem* **2010**, *11*, 2332−2336. (h) Tan, J. C.; Cheetham, A. K. *Chem. Soc. Rev.* **2011**, *40*, 1059−1080. (i) Spencer, E. C.; Kiran, M. S. R. N.; Li, W.; Ramamurty, U.; Ross, N. L.; Cheetham, A. K. *Angew. Chem., Int. Ed.* **2014**, *53*, 5583−5586.
(18) (a) Stroppa, A. *J. Phys. Conf. Ser.* **2013**, *428*, 012029/6. (b) Stroppa, A.; Barone, P.; Jain, P.; Perez-Mato, J. M.; Picozzi, S. *Adv. Mater.* **2013**, *25*, 2284−2290. (c) Di Sante, D.; Stroppa, A.; Jain, P.; Picozzi, S. *J. Am. Chem. Soc.* **2013**, *135*, 18126−18130.
(19) (a) Mączka, M.; Kadłubański, P.; Freire, P. T. C.; Macalik, B.; Paraguassu, W.; Hermanowicz, K.; Hanuza, J. *Inorg. Chem.* **2014**, *53*, 9615−9624. (b) Mączka, M.; Pietraszko, A.; Macalik, B.; Hermanowicz, K. *Inorg. Chem.* **2014**, *53*, 787−794. (c) Mączka, M.; Gągor, A.; Macalik, B.; Pikul, A.; Ptak, M.; Hanuza, J. *Inorg. Chem.* **2014**, *53*, 457−467. (d) Mączka, M.; Ptak, M.; Macalik, L. *Vibr. Spectrosc.* **2014**, *71*, 98−104.
(20) (a) Sanchez-Andujar, M.; Presedo, S.; Yanez-Vilar, S.; Castro-Garcia, S.; Shamir, J.; Senaris-Rodriguez, M. A. *Inorg. Chem.* **2010**, *49*, 1510−1516. (b) Pato-Doldan, B.; Sanchez-Andujar, M.; Gomez-Aguirre, L. C.; Yanez-Vilar, S.; Lopez-Beceiro, J.; Gracia-Fernandez, C.; Haghighirad, A. A.; Ritter, F.; Castro-Garcia, S.; Senaris-Rodriguez, M. A. *Phys. Chem. Chem. Phys.* **2012**, *14*, 8498−8501.
(21) (a) Kurmoo, M. *Chem. Soc. Rev.* **2009**, *38*, 1353−1379. (b) Dechambenoit, P.; Long, J. R. *Chem. Soc. Rev.* **2011**, *40*, 3249−3265. (c) Kurmoo, M.; Kumagai, H.; Chapman, K. W.; Kepert, C. J. *Chem. Commun.* **2005**, 3012−3014. (d) Kurmoo, M.; Kumagai, H.; Hughes, S. M.; Kepert, C. J. *Inorg. Chem.* **2003**, *42*, 6709−6722.
(22) Li, W.; Zhang, Z.; Bithell, E. G.; Batsanov, A. S.; Barton, P. T.; Saines, P. J.; Jain, P.; Howard, C. J.; Carpenter, M. A.; Cheetham, A. K. *Acta Mater.* **2013**, *61*, 4928−4938.
(23) Polyakov, A. O.; Arkenbout, A. H.; Bass, J.; Blake, G. R.; Meetsma, A.; Caretta, A.; van Loosdrecht, P. H. M.; Palstra, T. T. M. *Chem. Mater.* **2012**, *24*, 133−139.
(24) Kundys, B.; Lappas, A.; Viret, M.; Kapustianyk, V.; Rudyk, V.; Semak, S.; Simon, C.; Bakaimi, I. *Phys. Rev. B: Condens. Matter Mater. Phys.* **2010**, *81*, 224434/6.
(25) (a) Zhang, W.; Xiong, R. G. *Chem. Rev.* **2012**, *112*, 1163−1195. (b) Cai, H.-L.; Yi Zhang, L.; Fu, D.-W.; Zhang, W.; Liu, T.; Yoshikawa, H.; Awaga, K.; Xiong, R.-G. *J. Am. Chem. Soc.* **2012**, *134*, 18487−18490.
(26) (a) Mitzi, D. B. *J. Chem. Soc., Dalton Trans.* **2001**, 1−12. (b) Mitzi, D. B. *Prog. Inorg. Chem.* **1999**, *23*, 1−122. (c) Steadman, J. P.; Willett, R. D. *Inorg. Chim. Acta* **1970**, *4*, 367−371. (d) Arend, H.; Huber, W.; Mischgofsky, F. H.; Richter-van Leeuwen, G. K. *J. Cryst. Growth* **1978**, *43*, 213−223.
(27) (a) Manaka, H.; Yamada, I.; Nishi, M.; Goto, T. *J. Phys. Soc. Jpn.* **2001**, *70*, 241−247. (b) Kind, R.; Roos, J. *Phys. Rev. B* **1976**, *13*, 45−54. (c) Kind, R.; Blinc, R.; Zeks, B. *Phys. Rev. B* **1979**, *19*, 3743−3754. (d) Knorr, K.; Jahn, I. R.; Heger, G. *Solid State Commun.* **1974**, *15*, 231−238. (e) Heger, G.; Mullen, D.; Knorr, K. *Phys. Stat. Sol. A* **1976**, *35*, 627−637. (f) Geick, R.; Strobel, K. *J. Phys. C* **1977**, *10*, 4221−4239. (g) Arend, H.; Hofmann, R.; Waldner, F. *Solid State Commum.* **1973**, *13*, 1629−1632.
(28) (a) de Jongh, L. J.; Meidema, A. R. *Adv. Phys.* **1974**, *23*, 1−260. (b) Bellitto, C.; Day, P. *J. Mater. Chem.* **1992**, *2*, 265−271. (c) Day, P. *J. Chem. Soc., Dalton Trans.* **1997**, 701−705.
(29) Bramwell, S. T.; Holdsworth, P. C. W. *Phys. Rev. B* **1994**, *49*, 8811−8814.
(30) (a) Kimura, T. *Annu. Rev. Mater. Res.* **2007**, *37*, 387−413. (b) Tokura, Y.; Seki, S. *Adv. Mater.* **2010**, *22*, 1554−1565.
(31) (a) Efremov, D. V.; van den Brink, J.; Khomskii, D. I. *Nat. Mater.* **2004**, *3*, 853−856. (b) Mercone, S.; Wahl, A.; Pautrat, A.; Pollet, M.; Simon, C. *Phys. Rev. B* **2004**, *69*, 174433−174439. (c) Muñoz, A.; Alonso, J. A.; Martinez-Lope, M. J.; Casais, M. T.; Martinez, J. L.; Fernandez-Diaz, M. T. *Inorg. Chem.* **2001**, *40*, 1020−1028.
(32) Ghalsasi, P. S.; Inoue, K. *Polyhedron* **2009**, *28*, 1864−1867.
(33) (a) Kumagai, H.; Kepert, C. J.; Kurmoo, M. *Inorg. Chem.* **2002**, *41*, 3410−3422. (b) Kurmoo, M. *Philos. Trans. A* **1999**, *357*, 3041−3061. (c) Kurmoo, M.; Kumagai, H.; Green, M. A.; Lovett, B. W.; Blundell, S. J.; Ardavan, A.; Singleton, J. *J. Solid State Chem.* **2001**, *159*, 343−351.
(34) (a) Sheldrick, G. M. *Acta Crystallogr., Sect. A* **1990**, *46*, 467−473. (b) Sheldrick, G. M., *SHELXS-97, Program for X-ray Crystal Structure Solution*; University of Göttingen: Göttingen, Germany, 1997.
(35) (a) Brunskill, I. H.; Depmeier, W. *Acta Crystallogr., Sect. A* **1982**, *38*, 132−137. (b) van Arnstel, W. D.; de Jongh, L. J. *Solid State Commun.* **1972**, *11*, 1423−1429.
(36) de Jongh, L. J., Ed. *Magnetic Properties of Layered Transition Metal Compounds*; Kluwer Academic Publishers: Dordrecht, 1990; pp 1−51.
(37) Stanley, H. E. *Introduction to Phase Transitions and Critical Phenomena*; Clarendon Press: Oxford, 1991; pp 1−308.
(38) Bertotti, G. *Hysteresis in Magnetism*; Academic Press: London, 1998; pp 1−558.
(39) Herpin, A. *Theorie du Magnétisme*; Presse Universitaire de France: Paris, 1968; pp 1−882.

DOI: 10.1021/ic5030229
Inorg. Chem. 2015, 54, 2866−2874